Charge-driven structural transformation and valence versatility of boron sheets in magnesium borides

Yufeng Zhao, Chunmei Ban, Qiang Xu, Su-Huai Wei, and Anne C. Dillon

Phys. Rev. B **83**, 035406 — Published 14 January 2011

DOI: 10.1103/PhysRevB.83.035406

Charge-Driven Structural Transformation and Valence Versatility of Boron Sheets in Magnesium Borides

Yufeng Zhao, Chunmei Ban, Qiang Xu, Su-Huai Wei, Anne C. Dillon

National Renewable Energy Laboratory, Golden, Colorado 80401

ABSTRACT

Based on Density Functional Theory simulations, we have predicted a series of stable magnesium borides MgB_x with a broad range of stoichiometries, $2 < x \leq 16$, by removing magnesium atoms from MgB_2. The layered boron structures are preserved through an in-plane topological transformation between the hexagonal lattice domains and triangular domains. The process can be reversibly switched as the charge transfer changes with Mg insertion/extraction. The mechanism of such a charge-driven transformation originates from the versatile valence state of boron in its planar form. The discovery of these new physical phenomena suggests the design of a high-capacity magnesium boron battery.

The complexity of boron chemistry has already been demonstrated in boron clusters [1-8] and polymorphs [9] that display peculiar hybridization [10] and bonding behavior [11]. Recently, boron chemistry has been further enriched with the discovery of planar, tubular, and cage-like boron [12-18] as well as the prediction of metal boride nanotubes [19] and diamond-like boron [20], in which three-center (3-c) bonding has been shown to stabilize the two-center (2-c) backbone bonding analogous to carbon [14, 15, 21]. The demonstration of combined 3-c bonds (in a triangular lattice [22]) and 2-c

bonds (in a hexagonal lattice) in various planar forms [23] suggests that boron sheets exhibit highly versatile valence states. It is also practically important to note that both the layered structure [24] and versatility of valence [25] may enable a variety of new technologies including novel catalyst supports, tailored membranes or adsorbents as well as new ion insertion compounds relevant to energy storage and "smart" windows. Here we have chosen to examine the new boron material for a high energy density battery. Boron is superior to all previously known multi-valence materials, especially transition metal compounds, which are heavy, expensive, and often not benign.

The unique properties of B discussed above have inspired us to investigate: (i) how do the boron sheets respond dynamically to changes in their chemical environment, e.g., reducing metal density in the well-known magnesium boride MgB_2 [26, 27]; (ii) whether the layered structure of boron can be preserved when substantial quantities of Mg ions are removed from MgB_2, (iii) if so, how will the boron sheets transform their structures, and (iv) is the transformation reversible as the Mg ions are inserted and extracted?

To answer these questions, we focus here on a central reaction

$$Mg_MB_{2M} \rightleftharpoons Mg_NB_{2M} + (M - N)\,Mg, \qquad (1)$$

in which boron is involved as a layered structure, varying from a hexagonal sheet in MgB_2 (i.e., Mg_MB_{2M}, with M primitive unit cells simulated in a computational super cell) to sheets with mixed domains of hexagonal and triangular lattices in MgB_x (i.e., Mg_NB_{2M}, $x = 2M/N > 2$). In such a purposely designed reaction, many novel magnesium borides may be derived from MgB_2, through potentially reversible structural transformations of the boron sheets controlled by the B/Mg ratio (x). The feasibility of the reactions is evaluated by investigation of the energetics of the MgB_x compounds and the mechanism

of transformation of the boron sheets. The minimum energy pathway (MEP) of the reaction is also subsequently characterized.

We use the density functional theory method as implemented in the Vienna Ab initio Simulation Package [28]. A plane-wave basis set (400 eV cutoff) is employed in combination with an all-electron-like projector augmented-wave method. The local density approximation with the exchange-correlation functional parameterized by Perdew and Zunger [29] is also employed. For Mg, the chosen potential treats the semi core *p*-states as core states. We start with the optimization of the MgB_2, with Mg atoms intercalated between the hexagonal boron sheets parallel to the *x*-*y* plane and stacked periodically in the *z* direction. Periodic boundary conditions are applied to the unit cell in all three dimensions. To sample the Brillouin zone, 8×8×16 Monkhorst-Pack type **k**-point meshes are generated so that the total energy is well converged. The optimized lattice constants for the primitive unit cell of MgB_2, a = 3.039 Å and c = 3.454 Å, are in good agreement with experimental values, a = 3.086 Å and c = 3.524 Å [23, 24]. In simulation of the reaction expressed by Eq. (1), the smallest computational super-cell contains 4×4 primitive unit cells, that is, $M = 16$. Larger supper cells, where the size was doubled were also calculated. Although more possible Mg distribution patterns were predicted, we found that the lowest-energy structure is identical to the smaller cell simulations with a homogeneous Mg-ion distribution that minimizes Coulomb repulsion between the Mg ions. In addition, supercells that contain two B-layers in z-direction are used to check whether interlayer B-B bonds can form. For simplicity the smaller cells are discussed in detail below.

To test whether the sheet transformation can actually happen, we remove Mg atoms from the MgB_2 with the remaining atoms homogeneously distributed in the Mg

sublattice. The structures are then relaxed either via direct computational optimization or in molecular dynamics (MD) simulation. We find that the original hexagonal B-sheets spontaneously transforms in direct optimization when the metal density is equal to or lower than 1 Mg/8B (see animated illustrations in the supplemental EPAPS documents); at higher Mg density, the transformation is no longer spontaneous but takes place in the MD simulation at 300 K within 10 ps.

Figure 1 shows the atomic structures of borides Mg_4B_{32}, Mg_6B_{32}, Mg_8B_{32}, and $Mg_{12}B_{32}$, as projected to the B-sheet plane. All the intercalated Mg atoms are coordinated with hexagons. Although the sheet index η (defined by the percentage of the removed B atoms from the triangular sheet [23]) still applies, all the sheet structures studied here are directly transformed from the hexagonal sheet (after removal of a certain amount of Mg from MgB_2) through energy-minimizing simulation. We use symbols X(η) to describe sheet structures, where the letter X denotes structural similarity in symmetry and atomic arrangement. For example, E(1/5) and E(3/11) have identical rows of triangular structural units; H(7/39) has a hexagonal symmetry, whereas H′(9/41) has a slightly distorted hexagonal symmetry.

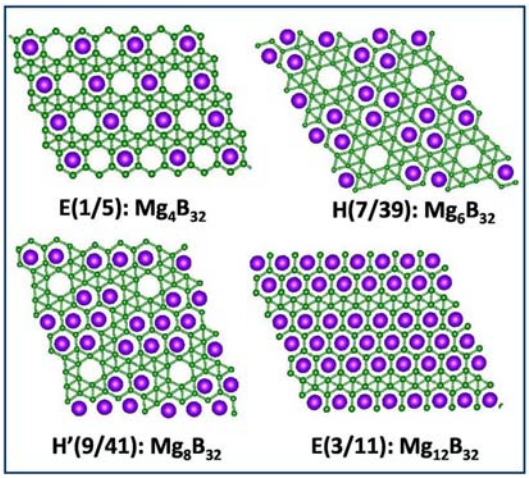

Figure 1. (Color on line) Atomic structures (projected in the *x*-*y* plane) of four magnesium borides derived from MgB_2 through reaction $Mg_{16}B_{32} \rightleftharpoons Mg_NB_{32} + (16 - N)$ Mg. The boron sheets are shown by web-like ball and sticks. The bigger balls (purple) denote Mg ions intercalated between the boron layers in the *z* direction. Four super cells are plotted for each case.

As previously reported, complex topological transformation can be decomposed into a sequence of single atomistic operations [25-27]. The same principle is true here and the underlying atomistic operation is consistently simplistic. Figure 2 (upper) shows the compressing plastic deformation (CPD) of a hexagon into four triangles, a basic process responsible for formation of all the structures (Fig. 1) out of the H(1/3) sheet. The reverse operation is a stretching plastic deformation (SPD). Such a reversible micro-process is extremely favorable for planar boron structures, which can adopt both the hexagonal 2-c and triangular 3-c bonding configurations, depending on the charge environment.

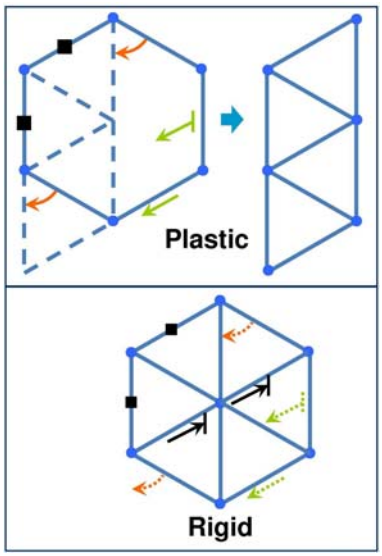

Figure 2. (Color on line) Upper panel: plastic deformation of a boron hexagonal lattice into a triangular lattice. Lower panel: rigidity of a seven-atom unit (SAU) with the hexagon decorated by an extra boron atom in the center. Squares, curved arrows and straight line arrows denote, respectively, freezing, rotation, and shift. Shielded arrows represent the blocking force.

However, for sheets containing the seven-atom units (SAU, Fig. 2), such as A(1/9), D(2/9), and F(1/4) described in Ref. [23], high rigidity prevents the compressive deformation from occurring. Note that none of the sheet structures transformed from the hexagonal sheet in this study has the rigid SAU structure (see Fig. 1). From a purely topological point of view, the SAUs combined with adjacent hexagons can be deformed into pentagon-heptagon pairs, which are transformable to hexagon domains through Stone-Wales bond rotation [30-32]. However, the pentagon-heptagon pairs have a much higher formation energy, according to our simulation. Therefore, transformation of the hexagonal sheet into A(1/9), D(2/9), or F(1/4) sheets is unlikely.

On the other hand, the sheets without an SAU—regardless of the difference from the H(1/3)—can eventually transform to the latter through a sequence of SPD/CPDs. For example, although the isolated rows of rhombic structural units in the G(3/10) sheet (Fig. 3a) appear incompatible with the hexagonal lattice, (Fig. 3h) they can still diffuse toward each other (Fig. 3 a→c→e), then combine (Fig. 3g), and eventually transform to an H(1/3) lattice (Fig. 3h). Each of the diffusion steps is achieved via propagating CPD/SPDs (i.e., Fig.3a→b, c→d, e→f). It should be pointed out that the coexistence of SPDs and CPDs requires local/temporal charge fluctuation because charge decreasing favors the CPDs and charge increasing favors the SPDs. When considering thermal diffusion of Mg ions,

local/temporal charge fluctuation is not a rare event. Therefore, the above transformation is probable.

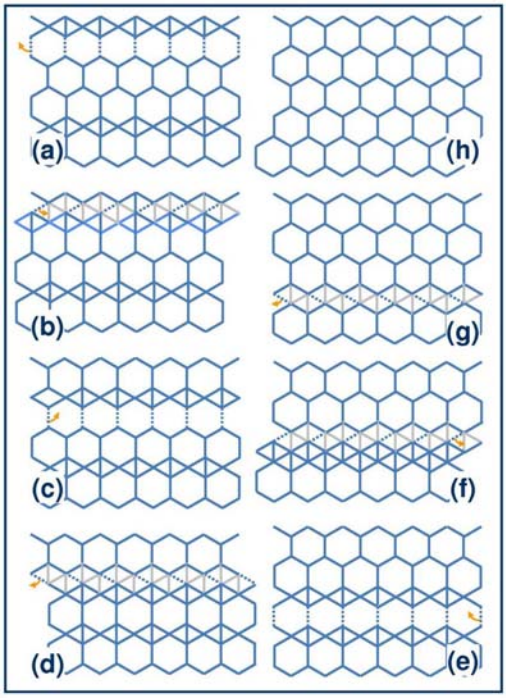

Figure 3. (Color on line) Transformation of G(3/10) to H(1/3) shown sequentially from (a) through (h). The dashed lines are bonds to be rotated following the arrows, after which the bonds shown in light gray will be broken. The portion above the dashed lines remains motionless, and the one below will be driven to shift by the bond rotation.

As we have seen, the CPDs driven by charge removal have rapid kinetics. Correspondingly, the SPDs driven by charge increase, upon metal insertion, are also rapid processes. To demonstrate this, we constructed an Mg_8B_{24} bulk structure with 24 B atoms in the unit cell of the H(1/7) sheet [23] and 8 intercalated Mg ions (Fig. 4c). The sheet transforms spontaneously into a G(1/4) structure (Fig. 4d) in the direct computational optimization (see the animation in the EPAPS documents). Obviously, the

G(1/4) can transform into E(1/4) if every two adjacent rows of rhombic structural units combine via the mechanism shown in Fig 3(e)-(g).

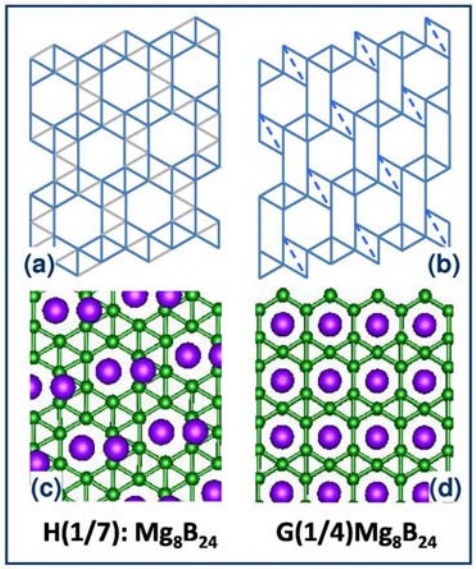

Figure 4. (Color on line) Lattice diagrams (a) and (b) show topological equivalence and transformability from H(1/7) to G(1/4) through SPDs: the light gray lines in (a) show bonds to be broken and the dashed lines in (b) show bond reconnections. The ball-and-stick models show the fully relaxed atomic structures of H(1/7) and G(1/4) for Mg_8B_{24}.

So far, eight sheet structures have been identified as fully transformable to hexagonal H(1/3) sheets via the CPD/SPD operations: G(3/10), E(3/11), G(1/4), E(1/4), H′(9/41), E(1/5), H(7/39), and H(1/7). In formation of magnesium borides, the density of intercalated Mg depends on the effective valence of boron, V_B, in these B-sheets, which can be defined by the charge transfer to per sheet atom required by the condition of optimal filling of the sheet orbitals [23]. According to Eq. (8) of Ref. [23], $V_B = -\frac{9\eta - 1}{3(1-\eta)}$ depends only on the sheet structure. The calculated valences for the

identified sheets are shown in Table I, varying from -1 for boron in MgB_2 [H(1/3)] to only -0.11 in H(1/7). This indicates that as the value of η decreases, the average coordination number per B increases, and the sheet is less electronegative. Based on the nominal valence of +2 for Mg, the minimum number of Mg atoms in the Mg_NB_{32} unit cell, N_{min}, required for saturated B-sheets can be derived (Table I). Our calculations show that further intercalation of Mg can still be energetically favorable if some hexagons are left uncoordinated with Mg. The maximum number of Mg per Mg_NB_{32} unit cell, N_{max}, is equal to the total number of hexagons in the B-sheet. Thus between $N_{\min}$ and $N_{\max}$, MgB_x with $x = 32/N$ is considered stable.

Table I. Effective B valence V_B in B-sheets, the minimum and maximum number of Mg atoms intercalated in a stable Mg_NB_{32}. For most of the boride structures, a unit cell with 32 B atoms is used, and the rest [i.e., H(1/7), G(3/10), and E(1/4) with 24, 28, and 24 B atoms per unit cell] are scaled to the formula of Mg_NB_{32}.

	H (1/3)	G(3/10)	E(3/11)	E(1/4)	H'(9/41)	E(1/5)	H(7/39)	H(1/7)
V_B	−1.00	−0.81	−0.67	−0.56	−0.42	−0.33	−0.25	−0.11
N_{min}	16.0	13.0	10.7	8.9	6.7	5.3	4.0	2.0
N_{max}	16.0	13.7	12.0	10.7	9.0	8.0	7.0	5.3

We have calculated the Mg binding energies $E = E_{tot}(Mg_NB_{32}) - N\mu_{Mg}$ (μ_{Mg} is the cohesive energy of Mg in bulk metal) in the Mg_NB_{32} compounds as a function of N. Two key features are observed in the upper panel of Fig. 5. *First*, the lowest-energy points of different Mg_NB_{32} structures fit to a straight line with good approximation. Because the

structures are obtained through energy-minimizing simulation, the straight line represents the energetic behavior of the MEP of reaction (1). *Second*, the N value of the Mg_NB_{32} that fall on the MEP is close to N_{min} and within the range $N_{min} < N < N_{max}$. We notice that as η increases, N_{min} approaches N_{max}. *Third*, the descending slope of the energy of the unsaturated Mg_NB_{32} becomes less steep as η and V_B decrease, and finally converges to the MEP line for small η. The lower panel of Fig. 5 shows that the energies of all Mg_NB_{32} at N_{min}. Although transformation of MgB_x with D(2/9) and F(1/4) sheets [23] to MgB_2 is unlikely, their minimum energy still falls close to the MEP.

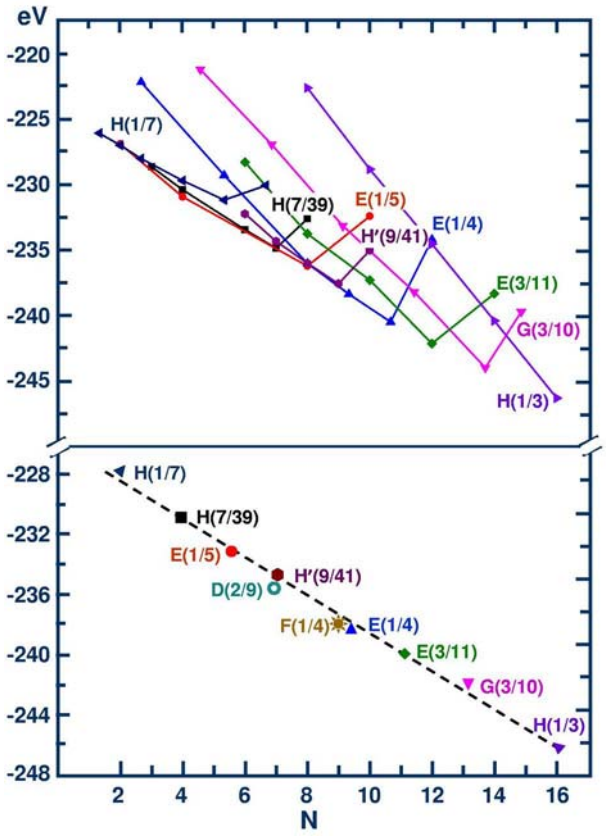

Figure 5. (Color on line) Energies of MgB_x (per Mg_NB_{32} unit cell) at various N (upper panel) and specifically N_{min} (lower panel). Because each computing unit cell of the G(3/10), E(1/4), and H(1/7) sheets has, respectively, 24, 28 and 24 boron atoms, their total energy and number of

Mg ions are scaled with respect to the Mg_NB_{32} formula, resulting in the non-integer N points.

Intriguing properties, such as superconductivity [27], have been discovered for magnesium boride MgB_2. Here we discuss its potential application for energy storage based on the versatile valence of boron sheets. Because the Mg ions play a key role in stabilization of the B-sheets, they should not be extracted completely in the electrochemical reaction. We found that buckling of the boron sheets and formation of interlayer B-B bonds only occur at a Mg density lower than that in Mg_4B_{32}. Therefore, we assume here 75% of the Mg ions can be reversibly extracted/inserted following the reaction cycle $12Mg + Mg_4B_{32} \rightleftharpoons Mg_{16}B_{32}$, the linear function $E_{tot}(N)$ of the MEP can give a constant output voltage of 0.64 V, or a binding energy of 1.28 eV/Mg. In this case, specific energy density of 561 Wh/kg (or 876 mAh/g) and volumetric density of 1550 Wh/L can be obtained from the computed total energy of -237.967 eV/Mg_4B_{32} for E(1/5), -274.397 eV/$Mg_{16}B_{32}$ for H(1/3), -1.758 eV/atom for Mg bulk, and the unit-cell volume of 362.40 $Å^3$ for E(1/5) and 441.47 $Å^3$ for H(1/3). The 22% volume expansion in the reaction is superior to an average 150% volume expansion in currently studied new Li-ion battery cathode/anode materials. Furthermore, good electronic and ionic conductivity are observed in all the MgB_x intercalation structures. None of them has a band gap and the smallest barrier of Mg-ion diffusion is around 0.8 eV at zero external electric field. Biased by the external voltage of 0.6-1.0 V, the ion diffusion barrier is expected to be lowered substantially.

Finally, to evaluate the stability of the predicted planar form of boron, we compared the total energy of the E(1/5): Mg_8B_{32} with the well-known cubic MgB_4

compounds [33] and found that the former is 0.21 eV/atom higher. Considering that the total energy of α-sheet is 0.4 eV/atom higher than the α-B_{12} bulk [20], the new planar form of boron is significantly stabilized in metal borides. Topologically, transformation of the planar boron to the cubic MgB_4 requires dramatic rearrangements of the atomic structure, therefore, must encounter much higher kinetic barrier than the nearly barrierless in-plan deformation.

The magnesium battery was first presented as an alternative to the lithium system [25], with advantages of safety, low cost, and higher energy density. However, the development of Mg-ion batteries is still subject to the major difficulty of achieving reversible distribution of the bivalent cations within the local crystal structure of an intercalation host. In our MgB_x system, this should not be a problem because the wide-range and continuous spectrum of valence states for boron sheets allows for extremely flexible exchange of multi-electrons, and the layered structures allow for fast, reversible insertion of Mg-ions. A similar principle has been recently proven [34] by using Cheverel phases (Mo_6S_8 or Mo_6Se_8), in which the polyvalent Mo_6 clusters have the capability to exchange up to 4 electrons. The relatively low output voltage of 0.64 V compared with 1.1 V for other cathode materials [34] may limit the application of the proposed Mg-B batteries, but importantly a high capacity has been predicted.

In conclusion, the planar form of boron exhibits a continuous spectrum of valence states. The origin of this unique property is the auto-transformation of the layered boron structures so that the average in-plane coordination number changes between 3 and 6. Due to this unique property, a variety of stable charge saturated magnesium borides MgB_x ($2 < x \leq 12$) can be formed. This also indicates that one may use Mg as a catalyst for the synthesis of new elemental boron phases or nanostructures. Also, our study

suggests that magnesium borides have high potential for high-capacity Mg-ion batteries. The versatility of the boron valence and mechanism of structural dynamics indicates superior chemical and mechanical properties, which are also foreseen in boron nanotubes and cages. In support of this exciting area established by the pioneering studies [11, 12], our calculations suggest that the structures of boron nanotubes/cages change with chemical environment thus enabling unique fundamental studies and applications to be explored.

This work was funded by the U.S. Department of Energy under subcontract number DE-AC36-08GO28308 through: DOE Office of Energy Efficiency and Renewable Energy Office of the Vehicle Technologies Program and NREL's Laboratory Directed Research and Development Program.

References

[1] R. N. Grimes, J. Chem. Edu. **81**, 658 (2004).
[2] I. Boustani, Phys. Rev. B **55**, 16426 (1997).
[3] E. D. Jemmis, and M. M. Balakrishnarajan, J. Am. Chem. Soc. **123**, 4324 (2001).
[4] E. D. Jemmis, M. M. Balakrishnarajan, and P. D. Pancharatna, J. Am. Chem. Soc. **123**, 4313 (2001).
[5] D. Prasad and E. D. Jemmis, Phys. Rev. Lett. **100**, 165504 (2008).
[6] W. Huang *et al.*, Nature Chemistry **2**, 202 (2010).
[7] E. Oger *et al.*, Angew. Chem. Intl. Ed. **46**, 8503 (2007).
[8] A. P. Sergeeva *et al.*, J. Am. Chem. Soc. **130**, 7244 (2008).
[9] D. A. Yang, *Phase Diagrams of the Elements* (Univ. of California Press, Berkeley, CA, 1991).
[10] A. R. Oganov *et al.*, Nature **457**, 863 (2009).
[11] M. Fujimori *et al.*, Phys. Rev. Lett. **82**, 4452 (1999).

[12] D. Ciuparu *et al.*, J. Phys. Chem. B **108**, 3967 (2004).

[13] B. Kiran *et al.*, Proc. Natl. Acad. Sci. U.S.A. **102**, 961 (2005).

[14] N. G. Szwacki, A. Sadrzadeh, and B. I. Yakobson, Phys. Rev. Lett. **98**, 166804 (2007).

[15] H. Tang, and S. Ismail-Beigi, Phys. Rev. Lett. **99**, 115501 (2007).

[16] T. T. Xu *et al.*, Nano Lett. **4**, 963 (2004).

[17] X. B. Yang, Y. Ding, and J. Ni, Phys. Rev. B **77**, 041402 (2008).

[18] H. J. Zhai *et al.*, Nature Materials **2**, 827 (2003).

[19] Y. Zhao *et al.*, Nano Lett. **8**, 157 (2008).

[20] Y. Zhao *et al.*, Chem. Phys. Lett. **496**, 280 (2010).

[21] A. Ceulemans *et al.*, Chem. Phys. Lett. **461**, 226 (2008).

[22] J. Kunstmann, and A. Quandt, Phys. Rev. B **74**, 035413 (2006).

[23] H. Tang, and S. Ismail-Beigi, Phys. Rev. B **80**, 134113 (2009).

[24] N. A. Chernova *et al.*, J. Mater. Chem. **19**, 2526 (2009).

[25] P. Novak, R. Imhof, and O. Haas, Electrochimica Acta **45**, 351 (1999).

[26] M. E. Jones, and R. E. Marsh, J. Am. Chem. Soc. **76**, 1434 (1954).

[27] J. Nagamatsu *et al.*, Nature **410**, 63 (2001).

[28] G. Kresse, and J. Furthmuller, Phys. Rev. B **54**, 11169 (1996).

[29] J. P. Perdew, and A. Zunger, Phys. Rev. B **23**, 5048 (1981).

[30] Y. F. Zhao, Y. Lin, and B. I. Yakobson, Phys. Rev. B **68**, 233403 (2003).

[31] Y. F. Zhao, R. E. Smalley, and B. I. Yakobson, Phys. Rev. B **66**, 195409 (2002).

[32] Y. F. Zhao, B. I. Yakobson, and R. E. Smalley, Phys. Rev. Lett. **88**, 185501 (2002).

[33] P. Villars, and L. D. Calvert, *Pearson's Handbook of Crystallographic Data for Intermetallic Phases, 2nd Ed.* (ASM International, Materials Park Ohio, 1991).

[34] E. Levi, Y. Gofer, and D. Aurbach, Chem. Mater. **22**, 860 (2010).